Passivity and Stability Boundaries for Haptic Systems with Time Delay

Thomas Hulin, Alin Albu-Schäffer, *Member, IEEE*, and Gerd Hirzinger, *Fellow, IEEE*

Digital Object Identifier: 10.1109/TCST.2013.2283372

URL: http://ieeexplore.ieee.org/xpl/articleDetails.jsp?arnumber=6648390

Passivity and Stability Boundaries for Haptic Systems with Time Delay

Thomas Hulin, Alin Albu-Schäffer, *Member, IEEE*, and Gerd Hirzinger, *Fellow, IEEE*

***Abstract*— This paper presents a passivity and a stability analysis of a one degree of freedom haptic device that is interacting with a virtual wall. These two analyses take into account the influence of a human operator and time delay. A peculiarity of the presented approach is the exact combination of discrete- and continuous-time elements, which reveals fundamental parameter dependencies for passivity and stability. These dependencies do not only differ in scale for passivity and stability, but consist in substantially different relations. By using realistic parameter ranges for human arms, this paper clearly illustrates that the maximum stable stiffness of virtual walls is far higher than admitted by passivity. Responsible for this great disparity is the limited stiffness of real human arms, as passivity covers a stiffness range that is orders of magnitudes larger than feasible. Finally, useful guidelines for designing stable haptic systems are concluded.**

***Index Terms*— Haptic rendering, passivity analysis, stability analysis, time delay.**

I. Introduction

HAPTIC force-feedback devices are typically used to display forces from virtual or distant environments to a human operator. For secure and efficient operation, haptic devices must never become unstable. A great challenge in analyzing stability of haptic interaction is taking into account the human operator's dynamics. Not only the diversity of human arm characteristics, but also the various possibilities of grasping haptic devices make it particularly difficult to determine a valid model of the human arm.

One approach of overcoming this problem is assuming passivity for the haptic device, and utilizing the fact that a human can always interact in a stable manner with a passive device. This idea is the basis for many theoretical control approaches in the field of haptics. Also Colgate and Schenkel [1] utilized this fact for deriving their famous passivity condition for haptic rendering. With their condition, a virtual wall can be parameterized in a passive way such that energy can never be extracted from the haptic system.

On the other hand, since this passivity-condition derived in the Laplace domain is conservative with respect to stability [1], [2], much higher stable stiffness values exist than admitted by passivity. Therefore, Hannaford, *et al.* [3] introduced a more accurate approach with their time-domain passivity controller. They introduced a variable damper, which eliminates the energy after it was generated by the haptic device. This approach was enhanced by different authors, e.g. [4]–[6].

In order to analyze the influence of nonlinear effects on passivity, Abbott and Okamura [7] investigated a haptic device that renders a simple virtual wall represented by a unilateral discrete-time spring, and included static friction and position quantization in their model. Their analysis revealed two restrictive conditions for the wall stiffness, one constituted by linear and the other by nonlinear effects. Both conditions must hold to obtain passivity. This finding was supported by more comprehensive analyses including time delay [8], or discrete-time damping [9]. These analyses indicate that the destabilizing nonlinear effect of sensor resolution can be compensated by other nonlinear effects, in particular static friction or dead-zone, and also motivate a separate investigation of linear effects.

A more recent theoretical approach [10] focuses on the linear effects while analyzing stability for haptic rendering including a mass-spring-damper model of the human arm. It compares the stable and passive parameter ranges of a virtual wall and states that the passive parameter region of undelayed haptic systems is a subset of the stable one. Although it focuses on the theoretical principles, experiments on three different haptic devices are confirming the validity of its stability analysis [11]–[13].

This paper extends this approach with respect to various aspects. Most importantly, it employs Colgate and Schenkel's general passivity condition [1] to derive passivity conditions for virtual walls including time delay as parameter, and compares the influence of each parameter with respect to the findings of the stability analysis. This paper is structured as follows. Section II describes the considered system and assumptions. Based on this system description, Section III investigated passivity and derives fundamental passivity conditions. Section IV summarizes previous work on the stability analysis [2], [10], [12] and introduces new findings and additions. Section V compares the results for passivity and stability and answers the following questions.

1) How do the passive parameter regions relate to the stable ones (Section V-A)?
2) How much is passivity restricting the virtual wall stiffness compared to stability (Section V-B)?
3) Why is passivity conservative in terms of stability (Section V-C)?

Finally, Section IV summarizes the main results and draws important conclusions for designing stable haptic systems.

Manuscript received November 16, 2012; accepted September 5, 2013. Manuscript received in final form September 23, 2013. Recommended by Associate Editor M. Fujita.

The authors are with the Institute of Robotics and Mechatronics, DLR, German Aerospace Center, Wessling 82234, Germany (e-mail: thomas.hulin@dlr.de; alin.albu-schaeffer@dlr.de; gerd.hirzinger@dlr.de).

Color versions of one or more of the figures in this paper are available online at http://ieeexplore.ieee.org.

Digital Object Identifier 10.1109/TCST.2013.2283372

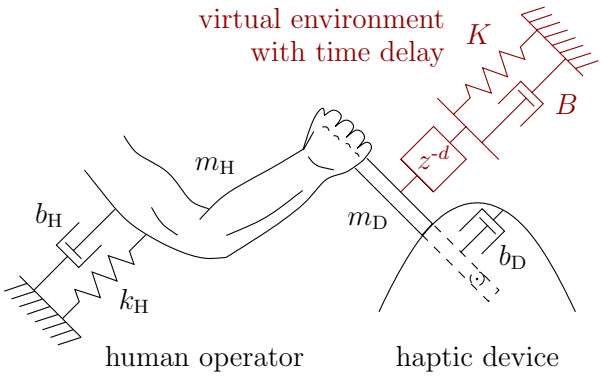

Fig. 1. Illustration of a human arm holding a one degree of freedom haptic device that is interacting with a delayed virtual wall.

II. System Description

In this paper, a system composed of a haptic device, a human arm, and a virtual environment including time delay is analyzed; see Fig. 1. For the passivity and stability analyses performed in the next sections, the following assumptions will be made on these system components.

A. Haptic Device

The haptic device is a single degree of freedom mass m_D, which is damped by a viscous damper b_D. It has constant sampling rate and constant time delay. Nonlinear effects like static friction, or quantization and saturation of sensors and actuators are not taken into account. Also the dynamics of the device actuators are neglected, such that a force F will be assumed to be applied constantly over one sampling period T. Furthermore, the device structure is assumed to be of high stiffness, such that structural compliance can be neglected.

B. Virtual World

For the virtual environment, the very common implementation as discrete-time spring-damper system (discrete-time PD-controller) is considered, with stiffness K and damping B. Thus, the transfer function of the virtual environment is

$$H(z) = K + B\frac{z-1}{Tz}. \tag{1}$$

The unilateral constraint of virtual walls is not considered for stability, although it can be shown that the passivity analysis in this paper also holds for such walls [1].

C. Time Delay

Considering the effect of time delay is crucial for the validity of any stability analysis on haptic interaction. This is, because each real haptic system is affected by time delay t_d, which may originate from different sources, including communication, force computation, or motor control. Due to the typically fast sampling rate of 1 kHz of haptic systems [14], a delay of only a few milliseconds means already a delay of several sampling steps T. Although a well-accepted design goal is keeping involved delays as small as possible, a few real haptic systems are affected by delays of clearly more than one sampling step, e.g., 5 ms [13].

Time delays in a closed control loop can be summarized without affecting the characteristic polynomial of a linear system. Therefore, without loss of generality, a combined time delay t_d is considered as the sum of all delays involved in the closed-loop of the haptic device and the virtual world. This delay is assumed to be constant and positive $t_d \geq 0$. It has a transfer function of $e^{-t_d s}$, or in the discrete-time domain z^{-d}, where d is the delay factor defined by $d = t_d/T$.

In comparison to standard discrete-time control theory, in which delay is defined as an integer multiple of the sampling period T, following calculations admit rational numbers for the delay factor $d \in \mathbb{Q}_{\geq 0}$. Rational delay factors typically occur in haptic systems with asynchronous read and write operations, or with delays in the motor controller. This extended definition is possible, since any discrete-time transfer function with rational delay factor can be transferred into a transfer function with a whole number for the delay factor by appropriately substituting the discrete-time variable z. Note that this approximation for rational delay factors considers discrete-time systems with multiples of the original sampling rate.

D. Human Arm

This paper uses two different models for the human arm. For the passivity analysis performed in the subsequent section, nearly no assumptions on the human operator have to be made, whereas the stability analysis requires a system model.

1) Stability: For the stability analysis in Section IV, the used model of the human arm is a single degree of freedom mass-spring-damper system, with mass m_H, stiffness k_H, and viscous damping b_H. This linear model of the real human has already been applied in many theoretical studies [15]. One reason therefore is obviously that it can be quite easily employed when analyzing stability of haptic systems, but more importantly, its validity could be supported by various experimental studies, e.g., [16]. It holds for small arm movements and time periods shorter than the time needed for humans to actively change their arm parameters. Hogan [17] found that for periods up to 1.2 s these parameters appear not to change.

Many different parameter values for the second-order arm model exist in literature [15]. This diversity originates from the different directions of movements considered, the posture of the user, as well as the individual's physical properties. Thus, for the stability analysis in this paper only limits for the parameter ranges of the fractions k_H/m_H, and b_H/m_H will be assumed, and not specific values of the three parameters. These limits will be introduced in Section IV.

It is further assumed that the human operator holds the haptic device in such a way that the human arm mass m_H is directly coupled to the device inertia m_D. Thus, the physical parameters of the haptic device and the human can be combined to

$$m = m_D + m_H \qquad b = b_D + b_H \qquad k = k_H \tag{2}$$

where m, b, and k are the effective physical mass, damping, and stiffness, respectively. Fig. 2 shows the physical equivalent of the addressed system.

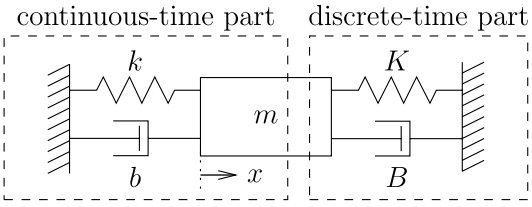

Fig. 2. Physical equivalent of the addressed system.

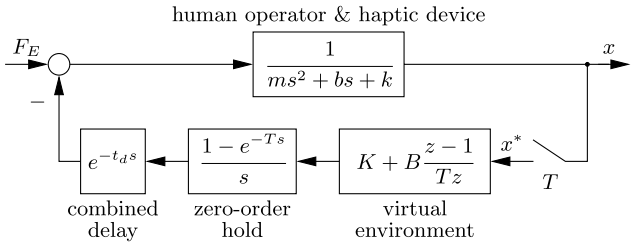

Fig. 3. Control loop of a haptic system employed for stability and passivity analysis.

With these assumptions, the control loop shown in Fig. 3 can be set up easily. It contains continuous-time (physical stiffness, damping, and mass) and discrete-time (virtual environment) elements. The input F_E is an external force, comprising the intended force of the human operator and possible collisions of the haptic device with the real environment. The calculations in Section IV assume this force being constant during a sampling period T, which may be considered as valid assumption, because the typical sampling rate of 1 kHz is much faster than the intended movements of a human [18].

2) Passivity: For the passivity analysis, no model of the human operator is used. It is only assumed that a human operator can interact stably with a passive haptic device, which corresponds to the assumption of Colgate and Schenkel in [1]. Thus, the considered physical system parameters are

$$m = m_\mathrm{D} \qquad b = b_\mathrm{D} \qquad k = 0. \tag{3}$$

However, the physical parameters of the human arm are implicitly taken into account in F_E, since the passivity analysis admits arbitrary changes of F_E, even during a sampling period T.

III. Passivity

Passivity is a physical system property that is often employed in control theory to guarantee stable behavior of complex systems. It has the appealing property that any interconnection of passive systems results in a passive and therefore stable overall system [19]. This section derives passivity boundaries for haptic rendering of delayed virtual walls, using the passivity condition introduced by Colgate and Schenkel in [1], which is based on mechanical energy using the conjugate power variables force and velocity. Their condition guarantees passivity for a haptic device interacting with a virtual environment with transfer function $H(z)$. It reads

$$b > \frac{T}{2}\,\frac{1}{1-\cos(\omega T)}\,\Re\{(1-e^{-j\omega T})H(e^{j\omega T})\} \tag{4}$$

for $0 < \omega < \omega_N$, where j the imaginary unit, and $\omega_N = \pi/T$ the Nyquist frequency. This condition also holds for virtual walls with a unilateral constraint.

A. Passivity Condition for Virtual Walls with Time Delay

Given the transfer function of the virtual environment (1) with time delay, the passivity condition (4) can be solved analytically for constant $d \geq 0$ using the equality for the exponential function for complex arguments $e^{x+jy} = e^x(\cos y + j \sin y)$, resulting in

$$\begin{aligned} b > \Big(&\big(\cos(d\cdot\omega T) - \cos((d+1)\omega T)\big)KT \\ &+\big(\cos(d\cdot\omega T) - 2\cos((d+1)\omega T) \\ &+\ \cos((d+2)\omega T)\big)B\Big)\Big/(2-2\cos(\omega T)) \end{aligned} \tag{5}$$

for $0 < \omega < \omega_N$. Note that this condition is independent of mass m. For $d = 0$, it results $b > KT/2 - B\cos(\omega T)$, which can be easily summarized as

$$b > \frac{KT}{2} + |B| \tag{6}$$

and which corresponds to the linear passivity condition for virtual walls without time delay, found by Colgate and Schenkel in [1].

B. Passivity Boundaries

In haptic simulations, the parameters of the virtual environment usually can be adapted more easily than those of the haptic device. Thus, it is helpful to draw the passivity boundaries in a parameter plane defined by K and B. The following lines solve the passivity condition (5) for these two parameters.

For a given damping b, delay d, and frequency ω, the passivity condition (5) is a line $l(b,d,\omega)$ in the (K,B)-plane. To determine an explicit representation of the passivity boundaries, two of these lines $l(b,d,\omega)$ and $l(b,d,\omega+\epsilon)$ must be crossed, with ϵ being an arbitrarily small positive quantity. Thus, the explicit representation results in

$$\begin{pmatrix} K \\ B \end{pmatrix} = 2b\cdot\begin{pmatrix} \frac{d+1}{T}\,\frac{\sin((d+2)\omega T)-2\sin((d+1)\omega T)+\sin(d\cdot\omega T)}{\sin(2(d+1)\omega T)-2(1+d)\sin(\omega T)} \\ \frac{d\cdot\sin((d+1)\omega T)-(1+d)\sin(d\cdot\omega T)}{\sin(2(d+1)\omega T)-2(1+d)\sin(\omega T)} \end{pmatrix}. \tag{7}$$

This equation reveals a linear dependency between the virtual wall parameters and the physical damping b, and additionally the sampling period T for K. Therefore, it is possible to draw the passivity boundaries in a (K,B)-plane normalized by b and T. Fig. 4 visualizes these boundaries for different delay factors d.

C. Boundary Analysis

The two limiting points of the passivity boundaries are $(K,B) = (0,b)$ and $(K,B) = (0,-b)$, independent of time delay d. The upper point at $B = b$ describes the point with the maximum possible passive virtual damping. It is reached

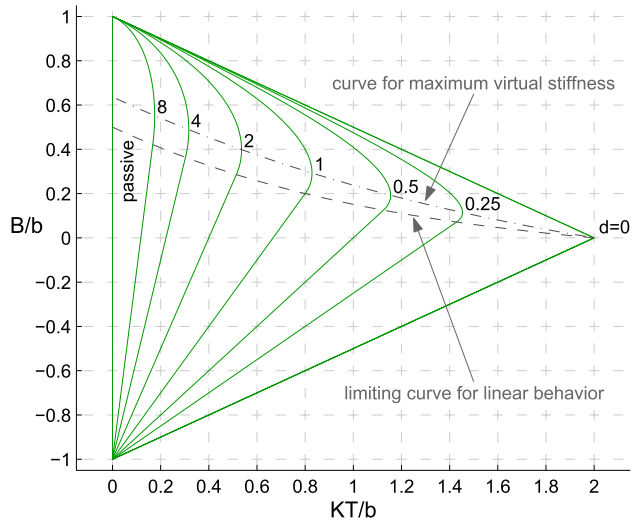

Fig. 4. Passivity boundaries of a haptic device rendering a virtual wall for different delay factors $d \in \{0, 0.25, 0.5, 1, 2, 4, 8\}$.

at a frequency $\omega|_{B_{\max}} = \pi / T(d+1)$ for a given delay d. At that frequency passivity condition (5) converges to the linear condition $b > KT/2 + B$, also independent of delay d. This condition corresponds to the upper part of the passivity boundary (6) for $d = 0$.

The lower parts of the passivity boundaries in Fig. 4 are linear. They can be derived as limits of the explicit passivity condition (7) at $\omega \to 0$ as

$$\begin{pmatrix} K \\ B \end{pmatrix}_{\text{lin}} = \begin{pmatrix} \frac{b}{T} \cdot \frac{6(d+1)}{(2d+1)(2d+3)} \\ b \cdot (\frac{d}{2d+3} + 1) \end{pmatrix} \cdot y + \begin{pmatrix} 0 \\ -b \end{pmatrix}, \quad y \in [0, 1] \quad (8)$$

which can be rewritten as

$$K < \frac{b+B}{(0.5+d)T}, \qquad \text{for } B \in \left[-1, \frac{d}{2d+3}\right] b. \quad (9)$$

If the effect of discrete-time sampling is assumed as a delay of half a sampling step $T/2$, which is a commonly used simplification in control theory, then this condition states that the virtual stiffness K must be smaller than the sum of dampings $b + B$ divided by the total delay $(0.5 + d)T$, or in other words

$$\text{Virtual Stiffness} < \frac{\sum \text{Damping}}{\sum \text{Delay}}. \quad (10)$$

As will be shown in the next section, this linear condition coincides with a linear condition for stability. The limiting curve of this linear part of the passivity boundary is plotted as a dashed line in Fig. 4.

For certain applications, it is interesting to know at which point the maximum virtual stiffness K can be reached. This point is the rightmost point on the passivity boundaries for given delay d in Fig. 4. In this point, the coefficient of the virtual damping B vanishes in passivity condition (5), which holds true for the frequency $\omega|_{K_{\max}} = \pi \ / \ 2T(d+1)$. Thus, the (K, B) value pairs for maximum possible passive virtual stiffness $K_{\max}$ results as

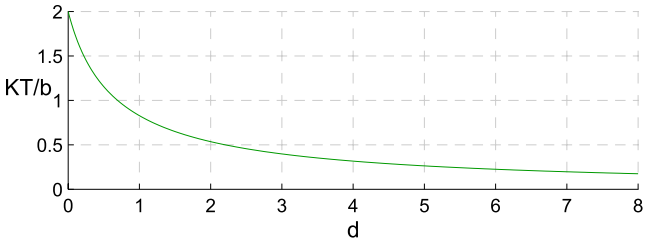

Fig. 5. Influence of the delay factor d on the maximum passive stiffness $K_{\max}$ in the normalized representation of Fig. 4.

$$\begin{pmatrix} K \\ B \end{pmatrix}_{K_{\max}} = b \cdot \begin{pmatrix} \frac{2}{T} \cdot \frac{1 - \cos(\frac{1}{2}\frac{\pi}{d+1})}{\cos(\frac{1}{2}\frac{\pi d}{d+1})} \\ \frac{\sin(\frac{1}{2}\frac{\pi d}{d+1}) - \frac{d}{d+1}}{\sin(\frac{1}{2}\frac{\pi}{d+1})} \end{pmatrix} \quad (11)$$

which is plotted as dash-dotted curve in Fig. 4. The influence of time delay d on $K_{\max}$ is illustrated in Fig. 5. Already for a delay of only one sampling step, i.e., $d = 1$, the maximum stiffness reduces to approximately 41% of its undelayed value, and for $d = 2$ less than 27% of the stiffness of the undelayed case can be reached.

IV. Stability

Previous Section derived a passivity condition and the passivity boundaries of a haptic device colliding with a virtual wall, while taking into account time delay. This Section derives stability boundaries for the same system, based on the results of [2], [10], and [12]. In contrast to the passivity analysis, where no model was needed, it assumes a linear model for the human operator with realistic parameter ranges.

A. Discrete-Time Equivalents

The considered system is the mixed discrete- and continuous-time system shown in Fig. 3. Thus, before performing a stability analysis of that system, all blocks of the control loop have to be transformed into a common time domain. The discrete-time domain is chosen, because calculating the exact discrete-time transfer function of the given system is straightforward [2], [20].

Since the mass-spring-damper system representing the human holding a haptic device and the delay are the only continuous-time blocks in the control loop in Fig. 3, only these blocks must be transformed into the discrete-time domain. The discrete-time equivalent of the delay is well known being $e^{-d\,Ts} \mathrel{\widehat{=}} z^{-d}$. The exact discrete-time equivalent of the mass-spring-damper system, can be determined by some calculations [2], while assuming the input force F_{E} being constant during one sampling period T, as shown in (12) at the bottom of the page, with

$$\begin{aligned} c_1 &= \sqrt{\left(\frac{bT}{m}\right)^2 - \frac{4kT^2}{m}} \\ c_2 &= e^{-(bT/m + c_1)/2} \\ c_3 &= e^{-(bT/m - c_1)/2}. \end{aligned} \quad (13)$$

TABLE I
NORMALIZATION RULES AND THE RESULTING DIMENSIONLESS PARAMETERS AS IN [10]

parameter	variable	dimensionless variable
sampling period	T	—
mass	m	—
delay	t_d	$d := t_d \,/\, T$
virtual stiffness	K	$\alpha := KT^2 \,/\, m$
virtual damping	B	$\beta := BT \,/\, m$
physical stiffness	k	$\gamma := kT^2 \,/\, m$
physical damping	b	$\delta := bT \,/\, m$

A system with these two equivalents has the exact same behavior at the sampling instants as the original system in Fig. 3.

TABLE II
POSSIBLE PARAMETER VALUES OF A HUMAN ARM (EXTENSION OF [15])

author(s)	m_H/kg	k_H/N/m	b_H/Ns/m
Daniel et al. [21][a]	1	39.5	12.6
Hogan [17]	0.8	568	5.5
Kazerooni et al. [22]	4.54	12.5	6.83
Kosuge et al. [23]	1.95	55	2.46
Kuchenbecker et al. [24]	0.15	1000	7.5
Lakatos et al. [25]	2.79	345	33.8
Lawrence [26]	17.51	175.1	175.1
Lawrence and Chapel [27]	0.5	40	6
Lee et al. [28]	0.15	7	0.5
Tsuji et al. [29]	1.8	199.1	26.2
Yokokohji et al. [30]	2.0	10.0	2.0

[a] This article considers a combined system of a human arm and a haptic device.

B. Normalized Characteristic Polynomial

Some of the parameters in discrete-time equivalent (12) can be grouped, such that a suited parameter substitution can simplify that formula. In [10] such a substitution is suggested, replacing all physical parameters by their dimensionless counterparts (see Table I). Inserting these substitution rules, the transfer function (12) becomes (14), as shown at the bottom of the page, with

$$\begin{aligned} c_1 &= \sqrt{\delta^2 - 4\gamma} \\ c_2 &= e^{-(\delta + c_1)/2} \\ c_3 &= e^{-(\delta - c_1)/2}. \end{aligned} \tag{15}$$

As now all elements of the investigated system in Fig. 3 are present in the discrete-time domain, its closed-loop transfer function can be set up easily. This transfer function from force F_{E}^* to position x^* results in

$$G_x(z) = \frac{T^2 z^{1+d}}{m} \cdot \frac{n(z)}{p(z)} \tag{16}$$

with

$$\begin{aligned} n(z) = {} & \left((c_2 + c_3 - 2)\, c_1 - (c_2 - c_3)\, \delta\right) z \\ & + \left(c_2 + c_3 - 2e^{-\delta}\right) c_1 + (c_2 - c_3)\, \delta \end{aligned} \tag{17}$$

and

$$\begin{aligned} p(z) = {} & \big((c_3 + c_2 - 2)c_1 + (c_3 - c_2)\delta\big)(\alpha + \beta)\, z^2 \\ & + \Big(\big((c_3 + c_2 - 2e^{-\delta})c_1 + (c_2 - c_3)\delta\big)\alpha \\ & \quad + \Big(+ 2\big((1 - e^{-\delta})c_1 + (c_2 - c_3)\delta\big)\beta\Big)\, z \\ & - 2\big(z^2 - z(c_3 + c_2) + e^{-\delta}\big)c_1\gamma\ z^{1+d} \\ & + \big((2e^{-\delta} - c_3 - c_2)c_1 + (c_3 - c_2)\delta\big)\beta \end{aligned} \tag{18}$$

where the force F_{E}^* and the position x^* are the discrete-time counterparts of the continuous-time signals F_{E} and x. It is important to note that the normalized characteristic polynomial $p(z)$ depends only on the five dimensionless parameters α, β, γ, δ, and d. The dependency of the mass m and the sampling time T is only implicit. Therefore, the trick with substituting the physical parameters transforms the original seven parameters system into a system with only five explicit parameters, which will drastically simplify the following stability analysis.

C. Parameter Range

The physical parameters involved in the system can strongly vary depending on the grasp of a human holding the haptic device. The range comprises from not holding the haptic device to holding it with full stiffness. Moreover, the physical parameters also highly depend on the direction of movement analyzed, as well as on the type of haptic device used. This Section determines realistic ranges for the two normalized physical parameters γ and δ, similar to [10]. To this end, the definitions of these two parameters are recalled first

$$\gamma = T^2 \cdot \frac{k_{\mathrm{H}}}{m_{\mathrm{D}} + m_{\mathrm{H}}} \qquad \delta = T \cdot \frac{b_{\mathrm{D}} + b_{\mathrm{H}}}{m_{\mathrm{D}} + m_{\mathrm{H}}}. \tag{19}$$

Assuming positive masses and dampers, these definitions can be used to derive the following two inequalities:

$$\gamma < T^2 \cdot \frac{k_{\mathrm{H}}}{m_{\mathrm{H}}} \qquad \delta < T \cdot \left(\frac{b_{\mathrm{D}}}{m_{\mathrm{D}}} + \frac{b_{\mathrm{H}}}{m_{\mathrm{H}}}\right). \tag{20}$$

Therefore, it is sufficient to determine independent upper limits for the human and the haptic device, to obtain conservative upper limits for γ and δ.

$$\frac{1}{ms^2 + bs + k} \mathrel{\widehat{=}} \frac{((c_2 + c_3 - 2)z + (c_2 + c_3 - 2e^{-bT/m}))(b^2 - 4km) + bc_1(c_3 - c_2)(z - 1)}{2k(z^2 - (c_2 + c_3)z + e^{-bT/m})(4km - b^2)} \tag{12}$$

$$\frac{1}{ms^2 + bs + k} \mathrel{\widehat{=}} \frac{T^2}{2m} \frac{\left((2 - c_2 - c_3)\, c_1 + (c_2 - c_3)\, \delta\right) z + \left(2e^{-\delta} - c_3 - c_2\right) c_1 + (c_3 - c_2)\, \delta}{c_1 \gamma \left(z^2 - (c_2 + c_3)\, z + e^{-\delta}\right)} \tag{14}$$

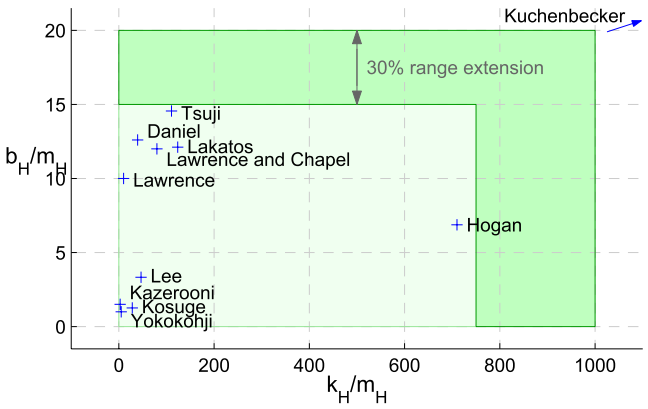

Fig. 6. Parameter values of the human arm of Table II normalized by the mass m_{H}. The parameter range considered in this paper for the stability analysis is extended by 30%.

Table II lists several values for mass, stiffness, and damping of human arms that were used in literature, comprising various grasps and different directions of movement. Fig. 6 shows the location of the fractions $k_{\mathrm{H}}/m_{\mathrm{H}}$ and $b_{\mathrm{H}}/m_{\mathrm{H}}$ for the values listed in that table. It appears that the fractions of Kuchenbecker *et al.* [24] are much higher compared to all the others, which is mainly due to two reasons.

First, in that study the arm was fixated by a strap, such that only the joint stiffness of the hand was measured. In contrast, the human arm stiffness results as series connection of many joint stiffnesses, and is therefore much smaller. Second, the human hand has better ratios of stiffness to mass, and damping to mass than the human arm, because its actuators (muscles) are located in the lower arm and therefore do not contribute to the hand mass. Due to these two reasons, these value pairs will be excluded when determining the parameter ranges.

For all the other values holds

$$\frac{k_{\mathrm{H}}}{m_{\mathrm{H}}} \leq 710\,\mathrm{s}^{-2} \qquad \frac{b_{\mathrm{H}}}{m_{\mathrm{H}}} \leq 14.6\,\mathrm{s}^{-1} \tag{21}$$

where s means seconds, and should not be mixed up with the Laplace variable s.

Normally, haptic devices are designed to exhibit very low physical damping, such that optimal haptic transparency (in the notion of Lawrence [26]) for unconstrained movements can be achieved easily. Diolaiti *et al.* [8] lists the parameters of several haptic devices. For all of them, the ratio of physical damping to mass $b_{\mathrm{D}}/m_{\mathrm{D}}$ is smaller than $0.625\,\mathrm{s}^{-1}$. With these findings, the following limits for the normalized parameters can be stated:

$$\begin{aligned} 0 \leq \gamma &< T^2 \cdot 710\,\mathrm{s}^{-2} \\ 0 \leq \delta &< T \cdot 15.225\,\mathrm{s}^{-1} \end{aligned} \tag{22}$$

if the cases of an ungrabbed device $k_{\mathrm{H}} = b_{\mathrm{H}} = 0$, and of an ideal undamped device $\delta = 0$ are also permitted. To account for the fact that reliable values for the physical parameters of human operators and haptic devices are in general quite imprecise values, parameter ranges extended by roughly 30% will be considered, see Fig. 6. Finally, it will be assumed that the sampling time T for haptic systems is limited from above at 1 ms, because this is a widely accepted limit for haptic rendering [14]. Therefore, the following parameter ranges will be considered

$$\begin{aligned} 0 \leq \gamma &\leq 1 \times 10^{-3} \\ 0 \leq \delta &\leq 20 \times 10^{-3}. \end{aligned} \tag{23}$$

Note that compared to [10], a wider range for δ is used, mainly because the values of Tsuji *et al.* [29] are added to Table II and thus are taken into consideration in this paper. The following section determines stability boundaries for these parameter ranges.

D. Stability Boundaries

Analytical solutions for stability could be found by using standard stability analysis methods, such as the Jury or the Routh-Hurwitz stability criterion [31]. These methods yield a set of inequalities. The stable parameter space is the intersection of the parameter spaces defined by these inequalities.

Since the characteristic polynomial (18) is of degree $d+3$, the analytical stability analysis quickly becomes quite complex for increasing delay d. An explicit solution for the case $d = 0$ and $\gamma = 0$, i.e., without time delay and physical stiffness, was derived by Gil *et al.* [15]. Already for a delay of $d = 1$, only an implicit solution could be determined [12]. Thus, for larger delays or non-zero stiffness γ, an iterative gridding method is used to determine the stable parameter space of the considered system.

This iterative method uses grid values of the investigated system parameters, and performs a stability check for each grid point by computing the zeros of the discrete-time characteristic polynomial function (18). At each transition from stable to unstable, or vice-versa, of two adjoining grid points, it determines a more precise numerical value by iterating the stability check on a finer grid, until a predefined threshold has been reached.

In analogy to the passivity boundaries, the stability boundaries are determined in the parameter plane of the virtual parameters, since these parameters are usually the parameters of a haptic system that can be changed most easily. Fig. 7 shows the stability boundaries in the normalized (α, β)-plane for a fixed delay $d = 0$, and for the limits of the possible parameter ranges of γ and δ, which were derived in previous subsection.

The stable regions have a vertical straight bound at $\alpha = -\gamma$. From the right side, i.e., for $\alpha > -\gamma$, they are bounded by parabola-like curves. As stated above, the analytical functions of these curves were derived only for $\gamma = 0$ and $d \in \{0, 1\}$, because for other cases the inequalities become very complex. When considering the normalization rule for α, it becomes obvious that the maximum stable virtual stiffness K depends quadratically on the sampling period T; a double sampling frequency with constant delay factor d (i.e., half time delay $t_d = d \cdot T$) enables a four times higher virtual stiffness K.

It is interesting to note that an increase of virtual damping does not automatically result in higher dissipation. Rather, as there is an upper bound for β, a too high virtual damping

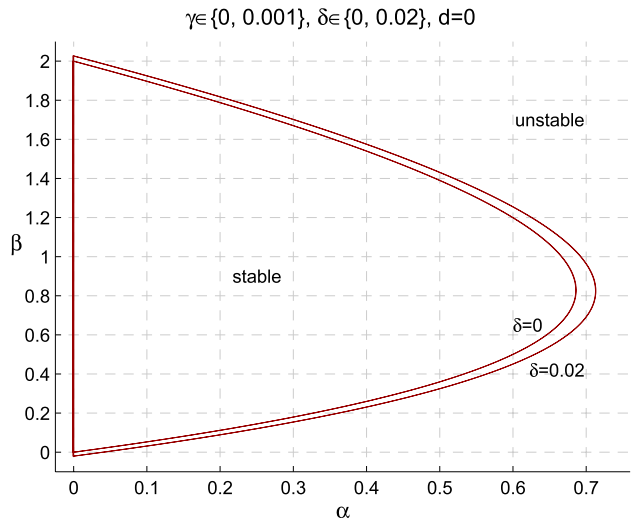

Fig. 7. Exact stability boundary in the (α, β)-plane for $d = 0$ and for the limits of the parameter range $\gamma \in [0, 0.001]$ and $\delta \in [0, 0.02]$. The effect of γ on the stability boundary is not visible in this scale.

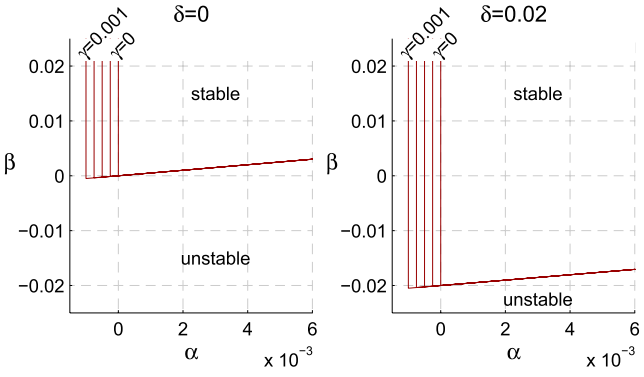

Fig. 8. Close-up of Fig. 7 around the origin, with additional values for γ, i.e., $\gamma \in \{0, 0.25, 0.5, 0.75, 1\} \cdot 0.001$. Physical stiffness γ is shifting the left boundary to $\alpha = -\gamma$ and not visibly influencing the bottom boundary.

itself can destabilize the system. This bound for the virtual stiffness B (as non-normalized parameter) depends linearly on the mass m and the sampling rate $1/T$.

On the other hand, physical damping δ increases the stable region toward each direction. Except the left vertical bound of the stable region is uninfluenced by δ. This bound is affected solely by the physical stiffness γ, which shifts it further to the left toward $\alpha = -\gamma$. This relationship is illustrated by the close-up views around the origin in Fig. 8. The influence of γ on the parabola-like part of the boundaries is rather marginal. Only for much higher stiffness values than admitted by the possible range $\gamma \gg 0.001$, the influence becomes clear, as will be detailed in the next section. For larger delays, the stable region becomes smaller (a detailed analysis can be found in [2] and [12]). Therefore, the influence of γ inside its bounds becomes visible in the overall shape of the stable region, see Fig. 9 for $d = 1$ and $d = 2$.

To conclude, physical stiffness and damping are increasing the stable region. Due to the normalization rules, which have the total (i.e., contributing human and device) mass m in

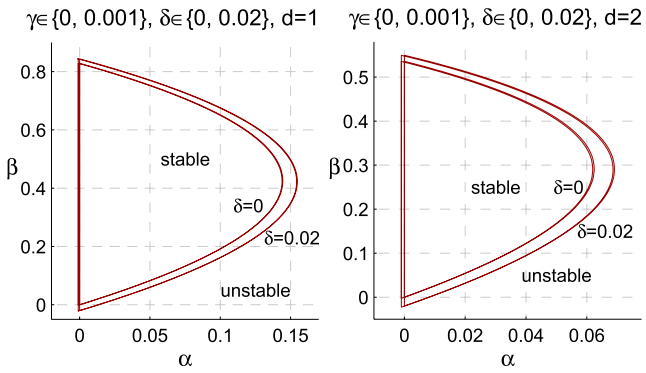

Fig. 9. Stability boundary in the (α, β)-plane for (left) $d = 1$ and (right) $d = 2$ for the limits of the parameter range $\gamma \in [0, 0.001]$ and $\delta \in [0, 0.02]$.

the denominator, also this mass contributes to stability, as it linearly scales the stable regions for the non-normalized parameters K and B. Therefore, if modeled as linear mass-spring-damper system, all three elements (the mass, the spring and the damper) of a human operator are stabilizing an impedance type haptic system.

E. Linear Stability Condition

When considering the virtual stiffness values typically employed in haptic simulations, it appears that for α usually small numerical values occur. For all devices listed by Diolaiti *et al.* [8], a value of $\alpha = 0.03$ is not exceeded. For such small values, the stability boundary can be linearized around the origin.

The resulting linear stability condition has been determined analytically in [10] and [12] by following procedure. First, the effect of sampling and hold and the time delay was approximated by a first-order lag element (PT1 element), and second, the Routh-Hurwitz criterion was applied on the resulting characteristic equation of the control loop. This criterion yields the linear stability condition as

$$K < \frac{b + B}{t_d + T/2}. \tag{24}$$

This condition corresponds precisely to the linear part of the passivity condition (9), but with physical damping being $b = b_\mathrm{D} + b_\mathrm{H}$. Note that the physical stiffness k does not influence condition (24), but shift the lower limit of the virtual stiffness to $K > -k$. In order to compare this linear approximation to the exact stability boundaries, it can be also expressed by normalized parameters

$$\beta + \delta > \alpha \left(\frac{1}{2} + d \right). \tag{25}$$

Fig. 10 shows the exact (solid) and this linear condition (dashed) in the same plots for values of the physical parameters that are inside the considered parameter range. As the influence of the physical stiffness in its admissible range on the stability boundaries is very small, this figure shows exemplarily the curves for the upper limit $\gamma = 0.001$. It visualizes also the points at which the relative error of the linear condition,

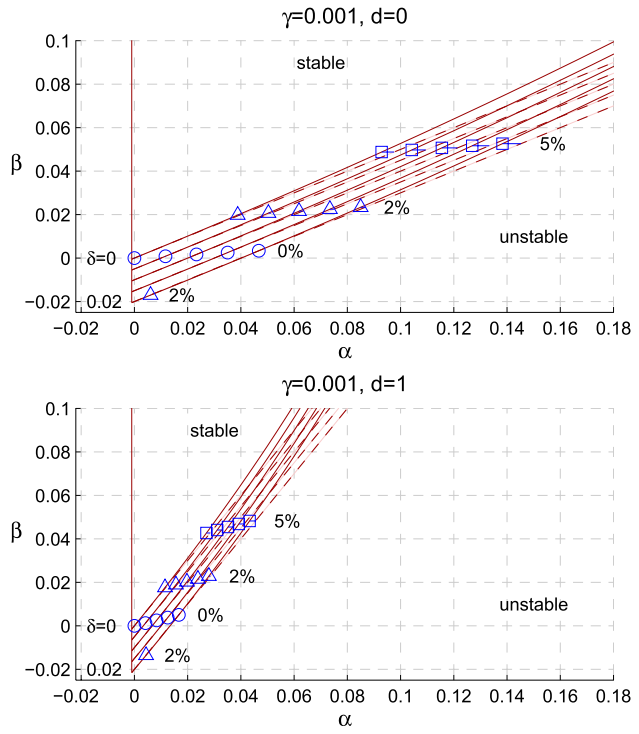

Fig. 10. Comparison of the linear stability condition (dashed lines) to the exact stability boundaries (solid lines), for $\gamma = 0.001$, $\delta \in \{0, 0.005, 0.01, 0.015, 0.02\}$, and $d = 0$ (top), respectively $d = 1$ (bottom). The relative error of the linear condition is marked in three levels, 0% (circles), 2% (triangles), and 5% (squares).

defined by

$$\left| \frac{\alpha_{\text{lin}} - \alpha}{\alpha + \gamma} \right| \tag{26}$$

reaches levels of 0% (circles), 2% (triangles), and 5% (squares). It appears that for damping values larger than $\delta > 0.015$, there are cases in which the relative error is larger than 2% also for negative β.

The linear condition crosses the stability boundaries at the points where the relative error is 0%, i.e., at the blue circles in Fig. 10. Above these crossing points, the linear condition is located on the unstable side of the stability boundary. Therefore, strictly speaking, the linear stability condition cannot be used to design stable control parameters for the virtual wall in this parameter range.

Although these new findings limit the use of the linear condition, this condition remains instructive with respect to the parameter dependencies for stability. In addition, for small values of the virtual damping $\beta \in [-1, d/(2d+3)]\delta$, the linear condition represents the linear part of the passivity boundary (9), such that in this parameter range the condition can be used to obtain even passive behavior.

V. Comparison Between Passivity and Stability

Above sections derived passivity and stability boundaries for the considered haptic system. This section compares both kinds of curves. Moreover, it relates the maximal virtual stiffnesses that can be achieved passively and stably. Finally, it analyzes stability for large values of physical stiffness, to build the bridge between stability and passivity.

A. Passivity and Stability Boundaries in the Same Figure

When applying the normalization rules for the dimensionless parameters of Table I, and assuming $m/T > 0$ the explicit representation of the passivity boundaries (7) becomes

$$\begin{pmatrix} \alpha \\ \beta \end{pmatrix} = \delta \cdot \begin{pmatrix} 2(d+1)\,\dfrac{\sin((d+2)\hat{\omega}) - 2\sin((d+1)\hat{\omega}) + \sin(d\cdot\hat{\omega})}{\sin(2(d+1)\hat{\omega}) - 2(1+d)\sin(\hat{\omega})} \\ 2\,\dfrac{d\cdot\sin((d+1)\hat{\omega}) - (1+d)\sin(d\cdot\hat{\omega})}{\sin(2(d+1)\hat{\omega}) - 2(1+d)\sin(\hat{\omega})} \end{pmatrix}. \tag{27}$$

for $\hat{\omega} = \omega T$ and $0 < \hat{\omega} < \pi$. Similarly to the stability analysis of previous section, the parameter sampling period T drops out also for passivity. This normalized equation defines the normalized passivity boundaries, which are proportionally scaled by the physical damping δ. For given δ and d, these boundaries can be plotted in the same (α, β)-plane as the stability boundaries. Fig. 11(a) shows both kinds of boundaries for $\gamma = 0.001$, $\delta = 0.02$, and $d \in \{0, 0.25, 0.5, 1, 2, 4, 8\}$. The dimensions of the passive regions are much smaller than those of the stable ones.

Thus, to present the passive regions more clearly, Fig. 11(b) shows a close-up view around the origin. This figure reveals that the passive region is a subset of the corresponding stable region for the given set of parameters, $\gamma = 0.001$, $\delta = 0.02$, and for time delays $d \geq 0$. This result is in accordance with the fact that the passivity condition is conservative in terms of stability [1].

The size of the passive regions is directly proportional to physical damping δ, whereas the relative dependency of the stable regions is much weaker (see previous section). In the shown case for $\delta = 0.02$, the passive regions are maximal for the considered parameter range. Thus, for smaller values of δ, the relative difference in size between the passive and the stable region becomes even larger.

B. Maximum Passive and Stable Stiffness

A fundamental requirement for a haptic system is that it is able to display a wide stiffness range. For soft contacts, the virtual stiffness can be decreased down to zero without causing stability problems. Yet, when increasing the virtual stiffness, stability becomes an issue. Thus, one important aspect of stability analyses for haptic systems is to handle the question, what maximal stiffness can be realized before the system becomes unstable. The following lines show how the maximum passive and stable stiffness change with increasing time delay, and compare the resulting two curves.

The maximum stable stiffness is given by the rightmost point on the stability boundary. When delay is changing, this point is moving with the boundary along a path with maximal stable stiffness. In Fig. 11(a), this path is plotted as a dash-dotted line, in analogy to the path for maximal passive stiffness, which was presented above in Fig. 4.

The difference of the maximum passive and stable stiffnesses becomes obvious, if they are both plotted in the

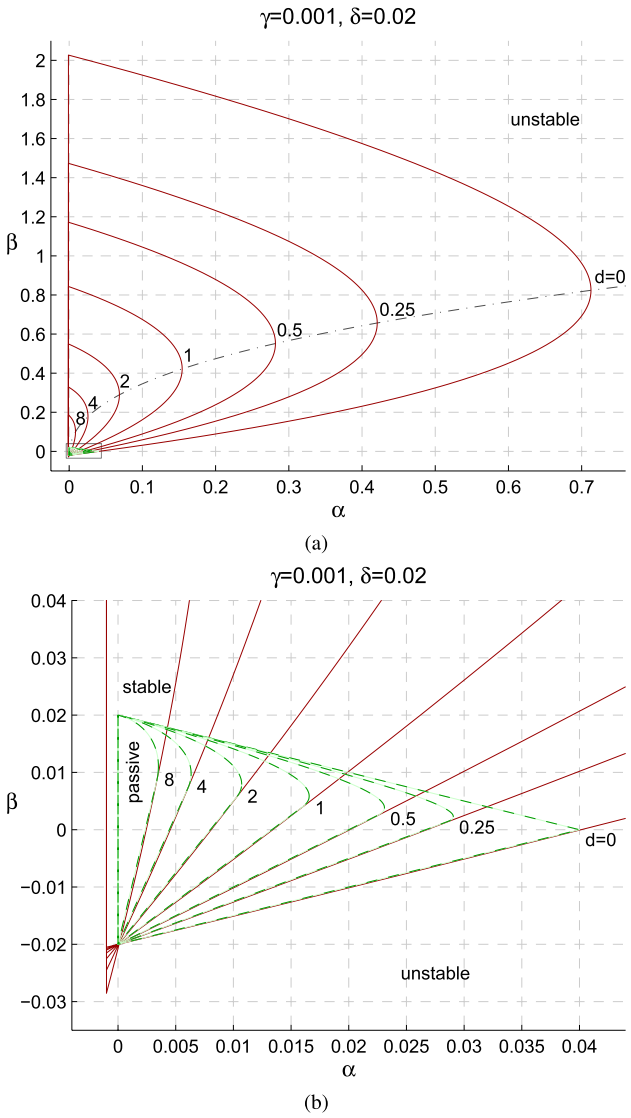

Fig. 11. Passivity boundaries (dashed green curves) and the stability boundaries (solid red curves) for $\gamma = 0.001$ and $\delta = 0.02$ in the same (α, β)-plane for different delay factors $d \in \{0, 0.25, 0.5, 1, 2, 4, 8\}$. The passive regions are inside the stable regions for a given delay. (a) Full view of the stability boundaries. The gray rectangle around the origin represents the close-up view of the plot below. (b) Close-up view around the origin.

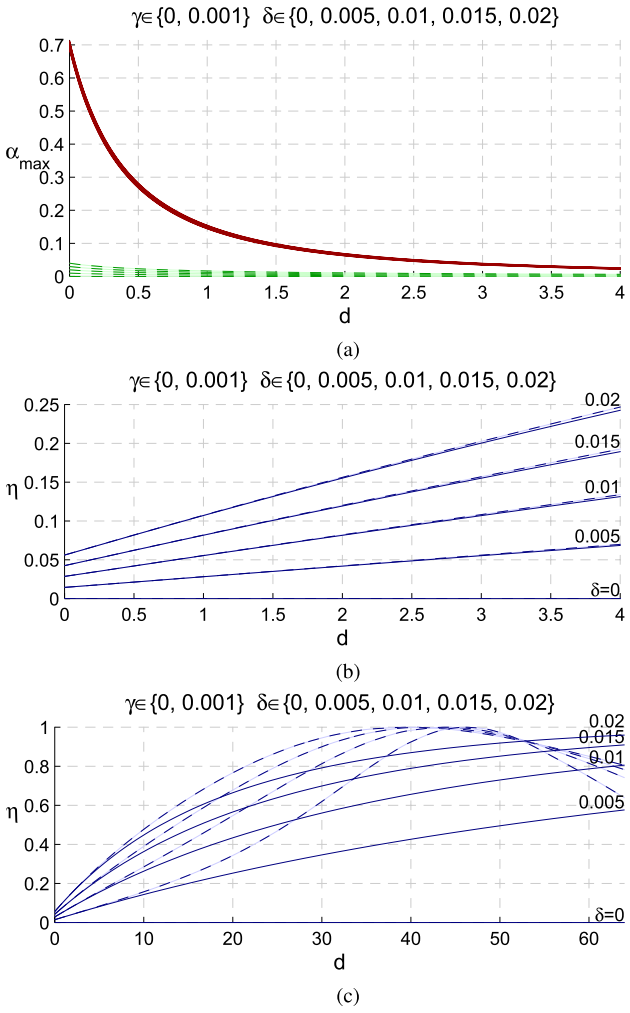

Fig. 12. Maximum virtual stiffness α for passivity and stability, and their ratio η. (a) Maximum virtual stiffness for passivity (dashed green curves) and stability (solid red curves). (b) Relation of maximum virtual stiffness for passivity and stability for $\gamma = 0$ (solid lines) and $\gamma = 0.001$ (dashed lines). (c) Relation of maximum virtual stiffness for passivity and stability for $\gamma = 0$ (solid lines) and $\gamma = 0.001$ (dashed lines).

same figure. Fig. 12 contains three plots that illustrate the dependency of these maximum values over the delay factor d. The first plot [Fig. 12(a)] shows directly the curves for these stiffness values. The maximum stable stiffness is clearly larger than the passive stiffness.

The lower two plots [Fig. 12(a) and (c)] illustrate the relation η of the maximum passive to the maximum stable virtual stiffness for two different scales of the delay factor d. They show that for increasing delay, the relation η becomes larger until the maximum passive and stable stiffnesses are the same at $\eta = 1$. This means that up to this point, the maximum stable stiffness depends higher on time delay than its maximum passive counterpart.

For $d = 0$, the maximum stable virtual stiffness is more than 17.8 times higher than achievable by passivity ($\eta_{d=0} < 0.0562$). If the delay increases to $d = 1$, this ratio decreases to values greater than 9.3 ($\eta_{d=1} < 0.1074$).

C. Passivity and Robust Stability

Up to here, a limited parameter range for the physical stiffness γ was considered, motivated by the stiffness that a human arm can apply. This subsection permits much larger values for γ, hence a connection between stable and passive regions can be found. The physical stiffness is influencing the oscillation frequency

$$\omega = \sqrt{\frac{k}{m} - \frac{b^2}{4m^2}}, \quad \text{for } k > \frac{b^2}{4m} \tag{28}$$

of the physical mass-spring-damper system given by the haptic device and the human operator. Substituting the physical by the normalized parameters yields

$$\omega = \frac{\sqrt{\gamma - \delta^2/4}}{T}. \tag{29}$$

Since the stability analysis in this paper is performed in the discrete-time domain, the oscillation of the mass cannot be observed correctly, if it exceeds the Nyquist frequency

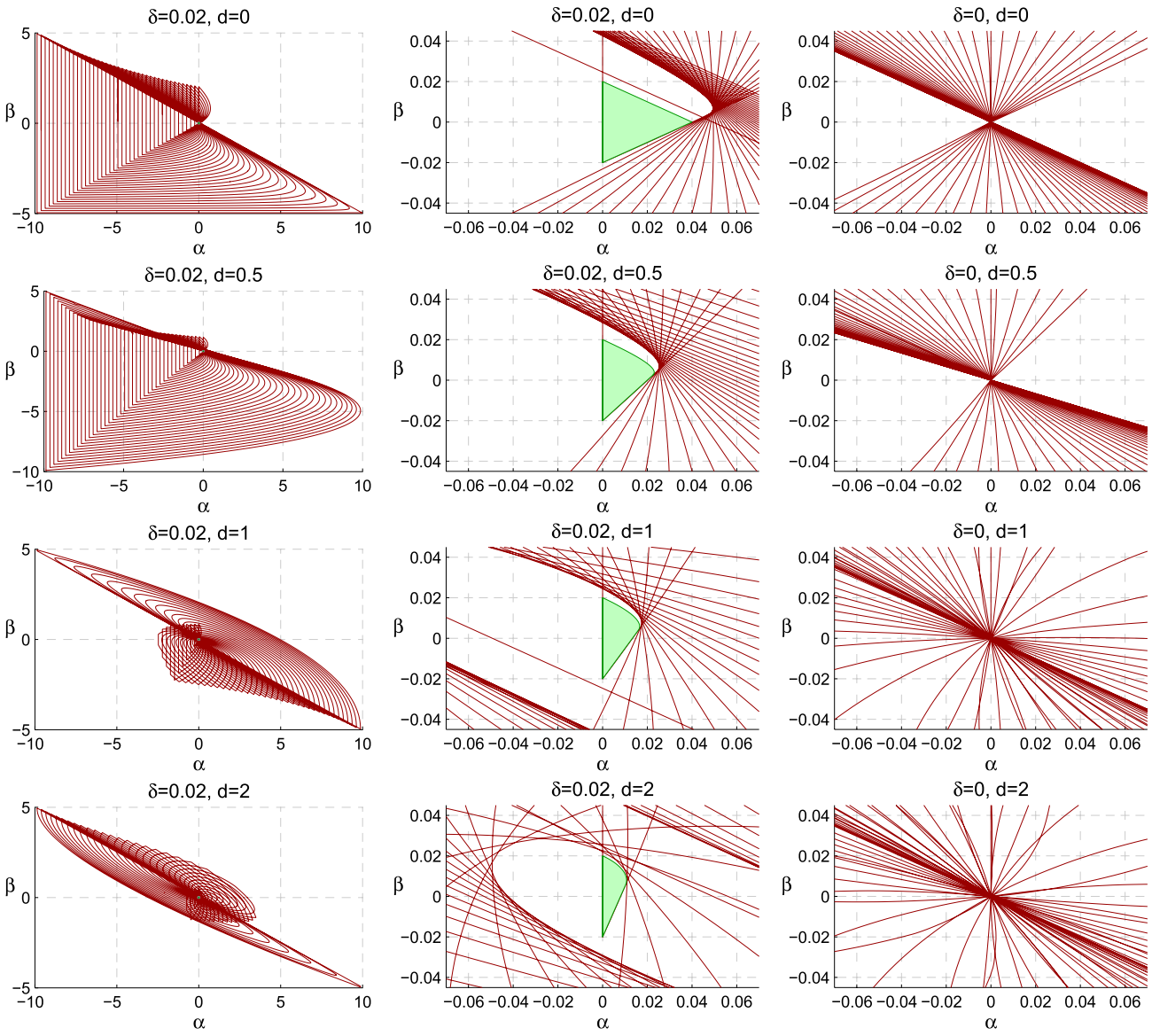

Fig. 13. Stability boundaries $\delta = 0.02$ and for parameter values of γ such that the system is reaching Nyquist frequency (left plots; $0 \leq \gamma \leq \pi^2 + \delta^2/4$). Close-up views are shown in the center and right plots for $\delta = 0.02$ and $\delta = 0$, respectively. The passive region is part of the robust stable region.

$\omega_N = \pi / T$. Therefore, this section investigates the stability of the haptic system for frequencies up to the Nyquist frequency

$$\gamma - \delta^2/4 \leq \pi^2. \tag{30}$$

With this condition and the possible parameter range for the physical damping $\delta \in [0, 0.02]$ results $\gamma \leq [\pi^2, \pi^2 + 0.0001]$ as limit for the physical stiffness. With previous assumption of a sampling frequency of at least 1 kHz, this limit is nearly 10 000 times larger than the maximum stiffness of a human arm defined in (23). Such high stiffness causes the stability boundaries to change completely their shape and size.

Example 5.1: To reach Nyquist frequency for an exemplary haptic device with parameters similar to the PHANToM haptic device [32], $m = 0.1\,\mathrm{kg}$ and $T = 0.001\,\mathrm{s}$, a physical stiffness of

$$k = \pi^2\, m / T^2 + b^2/4m \approx 987\,000\,\mathrm{N/m} \tag{31}$$

would be necessary, without considering mass of the human arm. Due to the square of the sampling period T in the denominator of the first summand, this stiffness value is only marginally influenced by the physical damping b. ■

Fig. 13 shows the stability boundaries for 41 evenly distributed values of γ between 0 and its maximum value $\pi^2 + \delta^2/4$, at which the Nyquist frequency is reached. This figure contains a row with three plots for each delay factor $d \in \{0, 0.5, 1, 2\}$. In each of these rows, the first plot on the left shows the overall shape of the stability boundaries for $\delta = 0.02$. Since the influence of the physical damping in its valid parameter range $\delta \in [0, 0.02]$ is hardly visible in this scale, the overall shape of the stability boundaries for $\delta = 0$ is not shown explicitly.

The second ($\delta = 0.02$) and the third ($\delta = 0$) plots in the middle and on the right, respectively, show close-up views around the origin. These plots reveal that there is an intersecting stable region for $\delta > 0$, which vanishes for $\delta = 0$

in the point of origin. Inside this intersecting region, the haptic system is robustly stable against the physical stiffness γ. In other words, a physical spring can never destabilize a haptic system, which is rendering a virtual wall with parameter values inside this intersection, independent of the spring stiffness.

Due to the definition of passivity, stating that energy can never be extracted from a system, the passive region must be part of the robustly stable region. Thus, the second plot also shows the passive region as green-shaded area, which confirms above statement. The passive region is located completely inside the robustly stable region independent of time delay and physical damping. Similar to the passive region, also the robustly stable region shrinks with increasing delay, and grows with increasing physical damping.

For $\delta = 0$, the whole stable region is limit stable at the Nyquist frequency $\gamma = \pi^2$, as the system has a pole at $z = -1$ independent of time delay d. For positive physical damping, $\delta > 0$ this pole moves inside the unit circle.

VI. Conclusion

This paper presents a passivity and a stability analysis on a one degree of freedom haptic device. The haptic device is interacting with a virtual environment represented by a discrete-time spring-damper system including time delay. The passivity analysis does not require any assumption on the human arm, whereas the stability analysis assumes the widely used linear mass-spring-damper model. For such a human model, the set of admissible human operator parameters was defined, taking into account various findings from other research groups.

The performed analyses result in passivity and stability boundaries in normalized parameter planes. For any time delay, the passive regions are completely contained in the stable regions. Both, the passive and the stable regions are highly affected by the delay involved in the haptic system. A delay of one sampling step decreases the maximum passive virtual stiffness to approximately 41% of its undelayed value. For stability, the dependency is even higher, such that a delay of one sampling period causes the maximum stable stiffness to decrease to less than 22% of the undelayed counterpart [as indicated by Figs. 11(a) and 12(a)].

Moreover, it is illustrated why passivity is conservative for haptic systems in terms of stability. Passivity considers a wide range of physical stiffness values, up to a stiffness that causes the system oscillating in frequencies close to the Nyquist frequency. Such high stiffness values are about 10 000 times larger than the maximally reachable stiffness of human arms.

A peculiarity of the presented approach is the exact combination of discrete- and continuous-time elements, which reveals fundamental parameter dependencies. These dependencies do not only differ in scale for passivity and stability, but are substantially different relations. The following lines detail the dependencies on the sampling rate, the physical damping, and the mass.

A faster **sampling rate** and accordingly less **delay** increases both, the maximum passive and stable stiffness. While the dependency of the passive stiffness is linear, the stable stiffness is quadratically depending on the sampling rate. In other words, for stability, two times faster sampling enables four times higher virtual stiffness. This implies that also the effective delay must be halved, as the analyses assume a constant delay factor.

The passive regions are proportional to **physical damping**, whereas an increase of damping is only marginally contributing to stability. This weak effect on stability can be explained by the numerically small values of physical damping, compared to the maximal stable virtual damping. Similarly, the effect of physical **stiffness** within the possible range is hardly affecting stability.

The moving **mass**, which is a combination of human arm and device mass, is proportionally scaling the stable region, while it has no influence on passivity. For stability, a doubling of mass enables a doubling of virtual stiffness and damping. However, as the performance of haptic systems is related to the fraction of stiffness to mass, higher stiffness does not lead to better performance, if mass increases equally.

From these dependencies, the following guidelines for designing stable haptic systems can be derived.

1) Try to minimize effective delay, composed of time delay and the phase shift caused by discrete-time sampling. A much faster sampling does not significantly improve performance, if time delay outweighs the effect of discrete-time sampling.
2) In order to improve haptic transparency, try to minimize physical damping, as it contributes only marginally to stability.
3) As a haptic device with very low mass is highly affected by the human mass, do not try to minimize the haptic device mass. This recommendation contrasts traditional design goals for haptic devices, which aim at maximizing haptic transparency. A sensible trade-off between transparency and stability might be designing devices for which the moving mass is in the range of the human mass contribution.

Further investigations analyzed the linear part of passivity boundaries. This part coincides with a linear approximation of the stability boundaries. Although this linear approximation has a small relative error over a wide range compared to the precise stability boundaries, it cannot be used to design stable system parameter values in general, because it is located partly outside of the stable region. Nevertheless, this linear approximation is very informative with regard to the relation of the involved system parameters. It states that the instability introduced by the product of stiffness and effective delay can be compensated by discrete- or continuous-time damping. In the range in which this linear approximation holds, discrete-time damping has the same dissipative behavior as its continuous-time counterpart.

The validity of the presented stability analysis has already been supported by experiments on three different haptic devices [11]–[13]. These experiments indicate a high correspondence between theory and practice, and thus confirm that

the assumptions made are valid. Nevertheless, as the systems used in these experiments were affected by delays of several sampling steps, more experiments on commercial haptic devices would reveal for which cases the theoretical results can be used, and when other factors—be it structural device elasticity, encoder resolution or other modeling inaccuracies—are causing instability.

ACKNOWLEDGMENT

The authors acknowledge the discussions and ideas of our former colleague Carsten Preusche. Moreover, the authors thank Philipp Kremer for the fruitful discussions.

REFERENCES

[1] J. E. Colgate and G. Schenkel, "Passivity of a class of sampled-data systems: Application to haptic interfaces," *J. Robot. Syst.*, vol. 14, no. 1, pp. 37–47, Jan. 1997.

[2] T. Hulin, C. Preusche, and G. Hirzinger, "Stability boundary for haptic rendering: Influence of physical damping," in *Proc. IEEE/RSJ Int. Conf. IROS*, Beijing, China, Oct. 2006, pp. 1570–1575.

[3] B. Hannaford and J.-H. Ryu, "Time-domain passivity control of haptic interfaces," *IEEE Trans. Robot. Autom.*, vol. 18, no. 1, pp. 1–10, Feb. 2002.

[4] J.-H. Ryu, C. Preusche, B. Hannaford, and G. Hirzinger, "Time domain passivity control with reference energy behavior," *IEEE Trans. Control Syst. Technol.*, vol. 13, no. 5, pp. 737–742, Sep. 2005.

[5] K. Hertkorn, T. Hulin, P. Kremer, C. Preusche, and G. Hirzinger, "Time domain passivity control for multi-degree of freedom haptic systems with time delay," in *Proc. IEEE ICRA*, Anchorage, AK, USA, May 2010, pp. 1313–1319.

[6] C. Ott, J. Artigas, and C. Preusche, "Subspace-oriented energy distribution for the time domain passivity approach," in *Proc. IEEE/RSJ Int. Conf. IROS*, San Francisco, CA, USA, Sep. 2011, pp. 665–671.

[7] J. J. Abbott and A. M. Okamura, "Effects of position quantization and sampling rate on virtual-wall passivity," *IEEE Trans. Robot.*, vol. 21, no. 5, pp. 952–964, Oct. 2005.

[8] N. Diolaiti, G. Niemeyer, F. Barbagli, and J. K. Salisbury, "Stability of haptic rendering: Discretization, quantization, time delay, and Coulomb effects," *IEEE Trans. Robot.*, vol. 22, no. 2, pp. 256–268, Apr. 2006.

[9] R. Iskakov, A. Albu-Schäffer, M. Schedl, G. Hirzinger, and V. Lopota, "Influence of sensor quantization on the control performance of robotics actuators," in *Proc. IEEE/RSJ Int. Conf. IROS*, San Diego, CA, USA, Oct. 2007, pp. 1085–1092.

[10] T. Hulin, C. Preusche, and G. Hirzinger, "Stability boundary for haptic rendering: Influence of human operator," in *Proc. IEEE/RSJ Int. Conf. IROS*, Nice, France, Sep. 2008, pp. 3483–3488.

[11] T. Hulin, J. J. Gil, E. Sánchez, C. Preusche, and G. Hirzinger, "Experimental stability analysis of a haptic system," in *Proc. Int. Conf. Enact. Inter.*, Montpellier, France, Nov. 2006, pp. 157–158.

[12] J. J. Gil, E. Sánchez, T. Hulin, C. Preusche, and G. Hirzinger, "Stability boundary for haptic rendering: Influence of damping and delay," *J. Comput. Inf. Sci. Eng.*, vol. 9, no. 1, pp. 011005-1–011005-8, Mar. 2009.

[13] T. Hulin, R. González Camarero, and A. Albu-Schäffer, "Optimal control for haptic rendering: Fast energy dissipation and minimum overshoot," in *Proc. IEEE/RSJ Int. Conf. IROS*, Tokyo, Japan, Nov. 2013.

[14] C. Basdogan and M. A. Srinivasan, "Haptic rendering in virtual environments," in *Handbook of Virtual Environments: Design, Implementation, and Applications*, K. Stanney, Ed. Boca Raton, FL, USA: CRC Press, 2002, pp. 117–134.

[15] J. J. Gil, A. Avello, A. Rubio, and J. Flórez, "Stability analysis of a 1 DOF haptic interface using the Routh-Hurwitz criterion," *IEEE Trans. Control Syst. Technol.*, vol. 12, no. 4, pp. 583–588, Jul. 2004.

[16] F. A. Mussa-Ivaldi, N. Hogan, and E. Bizzi, "Neural, mechanical, and geometric factors subserving arm posture in humans," *J. Neurosci.*, vol. 5, no. 10, pp. 2732–2743, Oct. 1985.

[17] N. Hogan, "Controlling impedance at the man/machine interface," in *Proc. IEEE ICRA*, vol. 3. Scottsdale, AZ, USA, May 1989, pp. 1626–1631.

[18] T. L. Brooks, "Telerobotic response requirements," in *Proc. IEEE Int. Conf. Syst., Man Cybern.*, Nov. 1990, pp. 113–120.

[19] R. Sepulchre, M. Janković, and P. V. Kokotović, *Constructive Nonlinear Control* (Communications and Control Engineering). London, U.K.: Springer-Verlag, 1997.

[20] N. K. Sinha, *Control Systems*. New Delhi, India: New Age International, 2008.

[21] R. W. Daniel and P. R. McAree, "Fundamental limits of performance for force reflecting teleoperation," *Int. J. Robot. Res.*, vol. 17, no. 8, pp. 811–830, Aug. 1998.

[22] H. Kazerooni, T.-I. Tsay, and K. Hollerbach, "A controller design framework for telerobotic systems," *IEEE Trans. Control Syst. Technol.*, vol. 1, no. 1, pp. 50–62, Mar. 1993.

[23] K. Kosuge, Y. Fujisawa, and T. Fukuda, "Mechanical system control with man-machine-environment interactions," in *Proc. IEEE ICRA*, May 1993, pp. 239–244.

[24] K. J. Kuchenbecker, J. G. Park, and G. Niemeyer, "Characterizing the human wrist for improved haptic interaction," in *Proc. 72nd ASME Int. Mech. Eng. Congr. Exposit.*, Washington, DC, USA, Nov. 2003, pp. 591–598.

[25] D. Lakatos, F. Petit, and P. van der Smagt, "Conditioning vs. excitation time for estimating impedance parameters of the human arm," in *Proc. IEEE-RAS Int. Conf. Humanoid Robots*, vol. 11. Bled, Slovenia, Oct. 2011, pp. 636–642.

[26] D. A. Lawrence, "Stability and transparency in bilateral teleoperation," *IEEE Trans. Robot. Autom.*, vol. 9, no. 5, pp. 624–637, Oct. 1993.

[27] D. A. Lawrence and J. D. Chapel, "Performance trade-offs for hand controller design," in *Proc. IEEE ICRA*, vol. 4. San Diego, CA, USA, May 1994, pp. 3211–3216.

[28] S. Lee and H. Lee, "Modeling, design, and evaluation of advanced teleoperator control systems with short time delay," *IEEE Trans. Robot. Autom.*, vol. 9, no. 5, pp. 607–623, Oct. 1993.

[29] T. Tsuji, Y. Takeda, and Y. Tanaka, "Analysis of mechanical impedance in human arm movements using a virtual tennis system," *Biol. Cybern.*, vol. 91, no. 5, pp. 295–305, Nov. 2004.

[30] Y. Yokokohji and T. Yoshikawa, "Bilateral control of master-slave manipulators for ideal kinesthetic coupling–formulation and experiment," *IEEE Trans. Robot. Autom.*, vol. 10, no. 5, pp. 605–620, Oct. 1994.

[31] H. Lutz and W. Wendt, *Taschenbuch der Regelungstechnik*. Frankfurt, Germany: Harri Deutsch, 2005.

[32] M. C. Cavusoglu, D. Feygin, and F. Tendick, "A critical study of the mechanical and electrical properties of the PHANToM haptic interface and improvements for high performance control," *Presence*, vol. 11, no. 6, pp. 555–568, 2002.

Thomas Hulin received the Dipl.-Ing. degree from the Technical University of Munich, Munich, Germany, in 2003.

He is with the Institute of Robotics and Mechatronics, German Aerospace Center (DLR), Wessling, Germany. He was involved in research on the development of the vibrotactile device VibroTac. His current research interests include haptic devices, control and algorithms, physical human-robot interaction, tele and space robotics, robot visualization, and skill transfer.

Mr. Hulin was a recipient of the DLR Innovation Award in 2012. He was a recipient of Conference Awards from the IEEE VR in 2012 and the HCI International in 2013.

Alin Albu-Schäffer received the M.S. degree in electrical engineering from the Technical University of Timisoara, Timisoara, Romania, in 1993 and the Ph.D. degree in automatic control from the Technical University of Munich, Munich, Germany, in 2002.

He has been the Head of the Institute of Robotics and Mechatronics, German Aerospace Center (DLR), Wessling, Germany, since 2012, which he joined as a Ph.D. candidate in 1995.

He is currently a Professor with the Technical University of Munich, holding the Chair for "Sensor-Based Robotic Systems and Intelligent Assistance Systems" with the Computer Science Department. He was involved in research on the development of the DLR light-weight robot and its commercialization through technology transfer to KUKA. His current research interests include robot design, modeling and control, nonlinear control, flexible joint and variable compliance robots, impedance and force control, physical human-robot interaction, and bioinspired robot design and control.

Prof. Albu-Schäffer was a recipient of several awards, including the IEEE King-Sun Fu Best Paper Award of the IEEE TRANSACTIONS ON ROBOTICS in 2012, several ICRA, and IROS Best Paper Awards as well as the DLR Science Award.

Gerd Hirzinger received the Dipl.-Ing. and Doctoral degrees from the Technical University of Munich, Munich, Germany, in 1969 and 1974, respectively.

He was with the German Aerospace Center (DLR), Wessling, Germany, in 1969, where he became the Head of the Automation and Robotics Laboratory, in 1976. In 1991, he received a joint professorship from the Technical University of Munich. From 1992 to 2012, he was the Director with DLR's Institute of Robotics and Mechatronics, which is one of the biggest and most acknowledged centers in the field worldwide, including not only robot development for space and terrestrial applications, but also aircraft control and optimization, vehicle technology, and medical. He has published more than 600 papers in robotics, mainly on robot sensing, sensory feedback, mechatronics, man-machine interfaces, telerobotics, and space robotics.

Prof. Hirzinger was a recipient of numerous high-ranked national and international awards.